J Biomol NMR (2007) 39:259–263
DOI 10.1007/s10858-007-9200-8

COMMUNICATION

Rapid measurement of $^{3}J(H^{N}–H^{\alpha})$ and $^{3}J(N–H^{\beta})$ coupling constants in polypeptides

Ravi Pratap Barnwal · Ashok K. Rout · Kandala V. R. Chary · Hanudatta S. Atreya

Received: 5 July 2007 / Accepted: 13 September 2007 / Published online: 4 October 2007

Abstract We present two NMR experiments, (3,2)D HNHA and (3,2)D HNHB, for rapid and accurate measurement of $^{3}J(H^{N}–H^{\alpha})$ and $^{3}J(N–H^{\beta})$ coupling constants in polypeptides based on the principle of G-matrix Fourier transform NMR spectroscopy and quantitative *J*-correlation. These experiments, which facilitate fast acquisition of three-dimensional data with high spectral/digital resolution and chemical shift dispersion, will provide renewed opportunities to utilize them for sequence specific resonance assignments, estimation/characterization of secondary structure with/without prior knowledge of resonance assignments, stereospecific assignment of prochiral groups and 3D structure determination, refinement and validation. Taken together, these experiments have a wide range of applications from structural genomics projects to studying structure and folding in polypeptides.

Keywords Coupling constants · GFT NMR · Protein Structures · Protein folding · Resonance assignment

The manuscript is dedicated to the memory of Late Bachimanchi Anjaneya Sastry, Former Professor and Head of the Department of Physics, University College of Science, Osmania University, Hyderabad, India 500 007.

Electronic supplementary material The online version of this article (doi:10.1007/s10858-007-9200-8) contains supplementary material, which is available to authorized users.

R. P. Barnwal · A. K. Rout · K. V. R. Chary (✉)
Department of Chemical Sciences, Tata Institute of Fundamental Research, Colaba, Mumbai 400005, India
e-mail: chary@tifr.res.in

H. S. Atreya (✉)
NMR Research Centre, Indian Institute of Science, Malleshwaram, Bangalore 560012, India
e-mail: hsatreya@sif.iisc.ernet.in

Three-dimensional (3D) structure determination of peptides and proteins by NMR spectroscopy benefits significantly from the measurement of three bond scalar coupling constants (^{3}J) (Wüthrich 1986). First, an improvement in the quality of structures results if the distance restraints derived from nuclear Overhauser effect measurements (NOEs) are supplemented by constraints derived from different three-bond coupling constants (Kim and Prestegard 1990; Garrett et al. 1994). Second, scalar coupling constants providing information on the backbone dihedral angle, ϕ, help in elucidating the secondary structure (Pardi et al. 1984; Wüthrich 1986). Third, measurement of such couplings aids in the stereospecific resonance assignments for prochiral protons which further improve the structure quality (Güntert et al 1989; Driscoll et al. 1989). To date, a number of NMR experiments have been proposed for the measurement of ^{3}J in polypeptides (Chary et al. 1991; Biamonti et al. 1994; Vuister et al. 1994). The 2D experiments proposed so far suffer from error in measurement of *J*-couplings due to chemical shift degeneracy, line-broadening and/or limited chemical shift precision. While degeneracy in chemical shifts can be reduced using 3D NMR experiments, their use in resonance assignment or/and structure determination is hampered by long 'minimal' measurement time required to acquire data with high digital resolution. We present here a set of G-matrix Fourier transform (GFT) NMR experiments overcoming these limitations and allowing rapid measurement of $^{3}J_{\mathrm{HNH}\alpha}$ and $^{3}J_{\mathrm{NH}\beta}$ in polypeptides. Rapid and accurate measurement of these coupling constants provides renewed opportunities to utilize them for: (i) resonance assignments, (ii) characterization of secondary structure with/without prior knowledge of resonance assignments, (iii) stereospecific assignment of prochiral groups and (iv) 3D structure determination and refinement.

GFT NMR spectroscopy (Kim and Szyperski 2003; Atreya and Szyperski 2005; Szyperski and Atreya 2006) is based on phase sensitive joint sampling of two or more chemical shifts in a single dimension, thereby providing high dimensional spectral information rapidly with high precision. GFT NMR has found several applications in protein resonance assignment and structure determination (Kim and Szyperski 2003; Atreya and Szyperski 2005). In the following, two GFT experiments are presented: (3,2)D HNHA (Fig. 1) and (3,2)D HNHB (Fig. 2) based on the method of quantitative *J*-correlation (Vuister et al. 1994) for measurement of $^{3}J_{\mathrm{HNH}\alpha}$ (Vuister and Bax 1993) and $^{3}J_{\mathrm{NH}\beta}$ (Dux et al. 1997), respectively. For the nuclei shown underlined, chemical shifts are jointly sampled (Kim and Szyperski 2003; Atreya and Szyperski 2005). Phase sensitive joint sampling of ^{15}N and ^{1}H chemical shifts is achieved by co-incrementing their respective chemical shift evolution periods with the ^{1}H shifts scaled by a factor 'κ' relative to ^{15}N (Szyperski and Atreya 2006). This results, after G-matrix transformation, in two sub-spectra each comprising of peaks at a given linear combination of chemical shifts along the indirect dimension: $\omega_1{:}\Omega(^{15}\mathrm{N}) \pm \kappa{*}\Omega(^{1}\mathrm{H}^{\alpha})$ and $\omega_1{:}\Omega(^{15}\mathrm{N}) \pm \kappa{*}\Omega(^{1}\mathrm{H}^{\mathrm{N}})$ in (3,2)D HNHA and $\omega_1{:}\Omega(^{15}\mathrm{N}) \pm \kappa{*}\Omega(^{1}\mathrm{H}^{\beta 2/\beta 3})$ and $\omega_1{:}\Omega(^{15}\mathrm{N}) \pm \kappa{*}\Omega(^{1}\mathrm{H}^{\mathrm{N}})$ in (3,2)D HNHB. The scaling factor, κ, allows one to increase the dispersion of peaks or to restrict the chemical shift evolution of ^{1}H to avoid loss in sensitivity due to transverse relaxation. A 2D [^{15}N, ^{1}H] HSQC

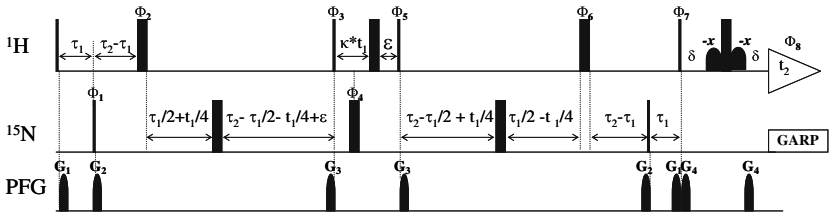

Fig. 1 R.f. pulse scheme of GFT (3,2)D HNHA. Rectangular 90° and 180° pulses are indicated by thin and thick vertical bars, respectively, and phases are indicated above the pulses. Where no r.f. phase is marked, the pulse is applied along *x*. High-power 90° pulse lengths are: 8.7 μs for ^{1}H, 37 μs for ^{15}N. κ = 0.5 (see text). The ^{1}H r.f. carrier is placed at the position of the solvent line at 4.7 ppm. The ^{15}N carrier position is set to 118.5 ppm. A WATERGATE sequence (Piotto et al. 1992) is used before the beginning of data acquisition for suppression of the residual water line using a Gaussian shaped ^{1}H r.f. pulse (Freeman 1998) of length 1.0 ms. GARP (Shaka et al. 1985) is employed to decouple ^{15}N (r.f. = 1.50 kHz) during acquisition. All pulsed z-field gradients (PFGs) are sine-bell shaped shaped with gradient recovery delay of 200 μs. The duration and strengths of the PFGs are: G1 (1.0 ms, 15 G/cm); G2 (1.0 ms, 22 G/cm); G3 (1.0 ms, 30 G/cm); G4 (1.0 ms, 10 G/cm). The delays are: τ_1 = 4.5 ms, τ_2 = 13.05 ms, ε = 43 μs and δ = 1.2 ms. Phase cycling: $\phi_1 = x$; $\phi_2 = 4(x),4(-x)$; $\phi_3 = x,-x$; $\phi_4 = 8(x)$, $8(-x)$; $\phi_5 = 2(x)$, $2(-x)$; $\phi_6 = 4(x),4(-x)$; $\phi_7 = y,-y$; ϕ_8 (receiver) = $8(x)$, $8(-x)$. Quadrature detection in $t_1(^{15}\mathrm{N})$ is accomplished by altering the phases ϕ_1 according to States-TPPI (Marion et al. 1989) (i.e., $\phi_1 = x,y$). GFT NMR phase-cycle: $\phi_3 = x$, y yields, in conjunction with quadrature detection in $t_1(^{15}\mathrm{N})$, 2 data sets which are linearly combined employing a G-matrix transformation (Kim and Szyperski 2003; Atreya and Szyperski 2005) with the G-matrix

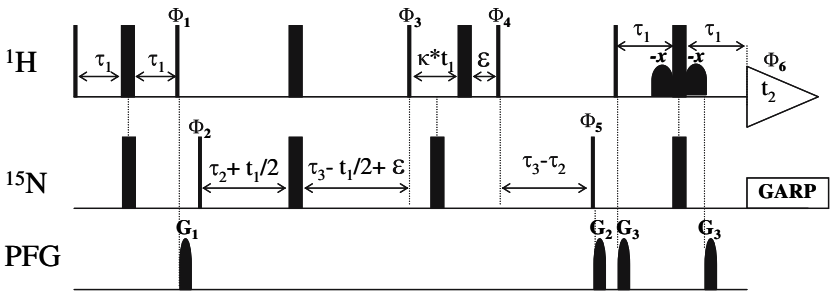

Fig. 2 R.f. pulse scheme of GFT (3,2)D HNHB. Rectangular 90° and 180° pulses are indicated by thin and thick vertical bars, respectively, and phases are indicated above the pulses. Where no r.f. phase is marked, the pulse is applied along *x*. High-power 90° pulse lengths are: 8.7 μs for ^{1}H, 37 μs for ^{15}N. κ = 0.5 (see text). The ^{1}H r.f. carrier is placed at the position of the solvent line at 4.7 ppm. The ^{15}N carrier position is set to 118.5 ppm. A WATERGATE sequence (Piotto et al. 1992) is used for suppression of the residual water line using a Gaussian shaped ^{1}H r.f. pulse (Freeman 1998) of length 1.0 ms. GARP (Shaka et al. 1985) is employed to decouple ^{15}N (r.f. = 1.5 kHz) during acquisition. All pulsed z-field gradients (PFGs) are sine-bell shaped with gradient recovery delay of 200 μs. The duration and strengths of the PFGs are: G1 (1.0 ms, 15 G/cm); G2 (1.0 ms, 30 G/cm); G3 (1.0 ms, 10 G/cm). The delays are: τ_1 = 2.3 ms, τ_2 = 4.0 ms, τ_3 = 31.9 ms, ε = 43 μs Phase cycling: $\phi_1 = y,-y$; $\phi_2 = 4(x),4(-x)$; $\phi_3 = 2(x)$, $2(-x)$; $\phi_4 = 4(x)$, $4(-x)$; $\phi_5 = 8(x)$, $8(-x)$; ϕ_6 (receiver) = $2(x,-x,-x,x)$, $2(-x,x,x,-x)$. Quadrature detection in $t_1(^{15}\mathrm{N})$ is accomplished by altering the phases ϕ_2 according to States-TPPI (Marion et al. 1989) (i.e., $\phi_2 = x$, y). GFT NMR phase-cycle: $\phi_3 = x$, y yields, in conjunction with quadrature detection in $t_1(^{15}\mathrm{N})$, 2 data sets which are linearly combined employing a G-matrix transformation (Kim and Szyperski 2003; Atreya and Szyperski 2005) with the G-matrix

provides central peak information (ω_1:$\Omega(^{15}N)$). In both (3,2)D HNHA and (3,2)D HNHB, the respective three-bond coupling constants are measured by taking the ratio of the intensity of peaks at $\Omega(^{15}N) \pm \kappa*\Omega(^{1}H^{\alpha/\beta})$ (equivalent to 'cross peaks' in the parent 3D experiment) to $\Omega(^{15}N) \pm \kappa*\Omega(^{1}H^{N})$ ('diagonal peak' in the parent 3D experiment). This ratio is proportional to a function of the corresponding scalar coupling constant (Vuister and Bax 1993; Dux et al. 1997).

The (3,2)D GFT NMR experiments presented here provide several advantages: (i) 3D spectral information can be obtained rapidly with good sensitivity (Table 1). (ii) Data are acquired with high spectral/digital resolution (Table 1). (iii) Spectra have high dispersion due to joint sampling of ^{15}N and ^{1}H shifts, which can be 'tuned' further by adjusting the scaling factor, κ. (iv) There are no 'diagonal' peaks due to detection of linear combination of ^{15}N and $^{1}H^{N}$ shifts. This allows integration of peaks which are otherwise difficult in the 3D experiment due to overlapping diagonal peaks (Vuister and Bax 1993).

In the present study, we acquired spectra for: (i) an u-^{15}N-labeled M-crystallin (predominantly a β-sheet protein; 9.5 kDa; 1.0 mM) (Barnwal et al. 2006) and (ii) an u-^{15}N-labeled calcium binding protein (*Eh*-CaBP; predominantly an α-helical protein; 16.2 kDa; 1.0 mM) (Atreya et al. 2001). These two systems were chosen to demonstrate the feasibility to different types/sizes of proteins and for the measurement of a varied range of coupling constants. The accuracy of measured couplings was assessed by comparing them with those predicted from the Karplus relationship (Karplus 1963) using their respective NMR-derived 3D structures. The accuracy was also evaluated by comparing the coupling constants with those measured using a regular 3D HNHA and 3D HNHB experiment. All NMR experiments were performed on Bruker Avance 700 MHz and 800 MHz spectrometers equipped with/without a cryogenic probe. The total measurement time for GFT spectra acquired ranged from 1.5 h to 6 h for (3,2)D HNHA and from 3 h to 14 h for (3,2)D HNHB (acquisition parameters are provided in Table 1).

Figure 3 shows the (3,2)D HNHA acquired for M-Crystallin (κ = 0.5). $^{3}J_{HNH\alpha}$ was measured for 77 out of an expected 80 residues (~96% yield; Table S1). Notably, a 3D HNHA with an *equivalent* spectral resolution would require 1–2 days for completion. For *Eh*-CaBP, data were recorded with κ = 1.0 to achieve higher spectral dispersion (Fig. S1). This yielded $^{3}J_{HNH\alpha}$ for 116 residues out of an expected 129 residues (~90% yield; Table S1; Fig. S1). Automatic calculation of the $^{3}J_{HNH\alpha}$ values was implemented using in-house written scripts. These scripts can be obtained from the authors upon request.

A comparison of measured $^{3}J_{HNH\alpha}$ couplings with those predicted from the 3D structures for residues in regular secondary structures is shown in Fig. 4. The accuracy of measured $^{3}J_{HNH\alpha}$ values are reflected in root mean square deviation (r.m.s.d.) of ≤ 1.0Hz obtained with the predicted couplings. For residues in regions with ill-defined conformation in the 3D structure, $^{3}J_{HNH\alpha}$ values were observed in range of 5.5–8 Hz (Fig. S3) reflecting motional averaging due to non-rigid backbone conformation. In addition, all $^{3}J_{HNH\alpha}$ values obtained from GFT spectra in M-Crystallin were compared with those obtained from a 3D HNHA,

Table 1 Acquisition parameters of NMR experiments

Sr. No.	Experiment[a]	Protein	Indirect dimension: t_{max} (ms); complex points; digital resolution (Hz/Pt)[b]	Spect. frequency (MHz)	Meas. time (h)	(S/N)[c] $\Omega(^{15}N) \pm \kappa*\Omega(^{1}H^{N})/\Omega(^{15}N) \pm \kappa*\Omega(^{1}H^{\alpha/\beta})$	Line-width[d] (ω_1) (Hz)	Peak detection yield (%)
1	(3,2)D HNHA	M-Crystallin	$\omega_1(^{15}N; ^{1}H)$: 25.0; 180; 7.2	800	1.5	18.5 ± 4.7/6.2 ± 2.3	21.6 ± 2.1/24.9 ± 2.3	94
			$\omega_1(^{15}N; ^{1}H)$: 32.0; 180; 5.5	700	3.0	34.0 ± 7.0/13.7 ± 5.1	23.2 ± 1.8/24.1 ± 1.2	95
		Eh-CaBP	$\omega_1(^{15}N; ^{1}H)$:32.0; 360; 5.5	700	6.0	36.3 ± 7.2/13.0 ± 8.6	26.5 ± 1.4/30.0 ± 3.0	90
2	(3,2)D HNHB	M-Crystallin	$\omega_1(^{15}N; ^{1}H)$: 25.0; 180; 7.2	800	3.0	10.2 ± 3.7/7.8 ± 3.2	22.9 ± 3.3/24.4 ± 2.4	88
			$\omega_1(^{15}N; ^{1}H)$: 32.0; 180; 5.5	700	6.0	8.7 ± 2.9/8.2 ± 3.5	22.5 ± 1.0/24.3 ± 1.6	91
		Eh-CaBP	$\omega_1(^{15}N; ^{1}H)$: 27.0; 200; 7.2	800	14.0	20.2 ± 6.8/20.8 ± 7.3	34.6 ± 2.1/39.3 ± 3.4	81
3	3D HNHA	M-Crystallin	$\omega_1(^{1}H)$: 9.0; 64; 9.7$\omega_2(^{15}N)$: 11.0; 20; 8.4	700[f]	12.0	17.7 ± 7.3/10.4 ± 3.8	82 ± 0.7/83 ± 0.8	84[e]
4	3D HNHB	M-Crystallin	$\omega_1(^{1}H)$: 6.0; 54; 9.7 $\omega_2(^{15}N)$: 12.0; 32; 8.4	800	18.0	24.1 ± 4.8/18.4 ± 5.6	139 ± 7/142 ± 6	86[e]

[a] A 2D [^{15}N, ^{1}H] HSQC was recorded as central peak spectra for M-Crystallin (~5 min) and *Eh*-CaBP (~5 min)

[b] Direct dimension $\omega_2(^{1}H^{N})/\omega_3(^{1}H^{N})$: 75; 512; 10.0

[c] S/N is calculated as ratio of the peak height to 2.5*standard deviation of the noise

[d] Line-widths for peaks at $\Omega(^{15}N) \pm \kappa*\Omega(^{1}H^{N})/\Omega(^{15}N) \pm \kappa*\Omega(^{1}H^{\alpha/\beta})$ are given

[e] Some of the peaks could not be integrated due to overlap of 'diagonal' peaks

[f] Data acquired using a conventional triple-resonance probe

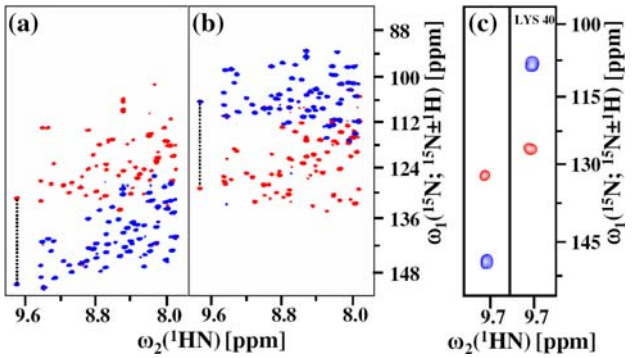

Fig. 3 (3,2)D HNHA acquired for M-crystallin showing signals at (**a**) ω_1:$\Omega(^{15}N) + \kappa^*\Omega(^1H)$ and (**b**) ω_1:$\Omega(^{15}N)–\kappa^*\Omega(^1H)$ (κ = 0.5). Peaks shown in blue and red correspond to $\Omega(^{15}N) \pm \kappa^*\Omega(^1H^N)$ and $\Omega(^{15}N) \pm \kappa^*\Omega(^1H^\alpha)$, respectively. (**c**) An expansion of peaks corresponding to Lys 40 (shown by dotted lines in panels **a** and **b**)

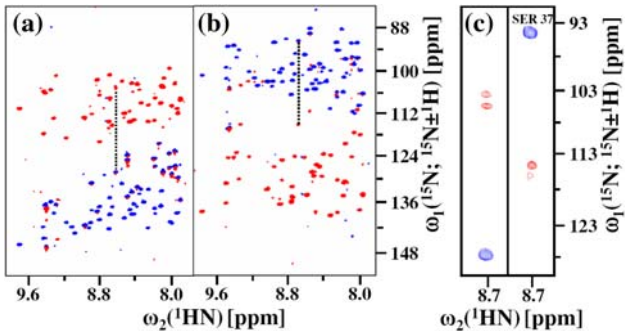

Fig. 5 (3,2)D HNHB of M-crystallin showing signals at (**a**) ω_1:$\Omega(^{15}N) + \kappa^*\Omega(^1H)$ and (**b**) ω_1:$\Omega(^{15}N)$-$\kappa^*\Omega(^1H)$ (κ = 0.5). The peaks shown in blue and red correspond, respectively, to $\Omega(^{15}N) \pm \kappa^*\Omega(^1H^N)$ and $(\Omega(^{15}N) \pm \kappa^*\Omega(^1H^{\beta2/\beta3}))$. (**c**) An expansion of peaks corresponding to Ser 37 with non-degenerate $^1H^{\beta2/\beta3}$ chemical shifts (shown by dotted lines in panels **a** and **b**)

giving an r.m.s.d. of 0.6 Hz (Fig. S4). This suggests an error of ~0.4 Hz for couplings measured in the GFT spectra (Assuming both GFT and its 3D congener have similar errors in couplings, r.m.s.d = $\sigma^*\sqrt{2}$, where σ denotes the error of couplings measured).

Figure 5 shows the (3,2)D HNHB acquired for M-Crystallin. $^3J_{NH\beta}$ were measured for 104 out of an expected 114 couplings (Table S1). In conjunction with NOE data, this helped in the stereospecific assignment of 30 out of 46 β-methylene proton pairs with non-degenerate shifts. In addition, rotamer conformation for all the 14 Val/Ile/Thr residues was obtained. In the case of *Eh*CaBP, $^3J_{NH\beta}$ were measured for 161 out of an expected 198 couplings from the (3,2)D HNHB (Table S1; Fig. S2).

It is known that $^3J_{HNH\alpha}$ (through its relation to ϕ) correlates with secondary structure in polypeptides (Pardi et al. 1984; Wüthrich 1986). Thus, the rapid measurement of $^3J_{HNH\alpha}$ using (3,2)D HNHA can facilitate a quick estimation of secondary structure content without prior knowledge of sequence specific resonance assignments. This was verified in the case of M-crystallin and *Eh*CaBP by counting spin-systems that have $^3J_{HNH\alpha}$ in the range of <5.5 Hz (α-helix), 5.5–8.0 Hz/unobserved residues (random-coil) and >8.0 Hz (β-sheet). The fraction of residues in these ranges were ~19%, ~41%, ~40% for M-Crystallin and ~54%, ~35%, ~11% for *Eh*-CaBP correlating well with their secondary structure (α-helix, random-coil, β-sheet) content of ~12%, ~40%, ~48% and ~57%, ~34%, ~9%, respectively, based on their chemical shift indices (Wishart and Sykes 1994) and 3D structures (Figs. 2, S3). Thus, (3,2)D HNHA can benefit: (i) structural genomics projects where samples are screened to evaluate feasibility for pursuing crystallization/NMR studies (Montelione et al. 2000; Page et al. 2005), (ii) protein-folding studies probing secondary structures in different states (Dyson and Wright 2004), and (iii) automated assignment methods utilizing information on secondary structure (Choy et al. 1997; Baran et al. 2004). On the other hand, (3,2)D HNHB provides $^1H^\beta$ shifts rapidly, which together with C^α and C^β shifts, can aid in spin system identification for resonance assignments (Atreya et al. 2000). Further, $^3J_{NH\beta}$ in the case of Ile, Thr and Val provides information on their corresponding χ_1 torsion angle. Taken together, these experiments provide

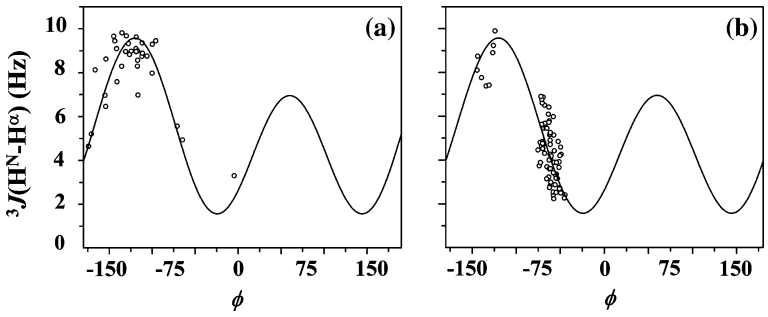

Fig. 4 Plot of $^3J_{HNH\alpha}$ for (**a**) M-crystallin, (**b**) *Eh*-CaBP as a function of ϕ obtained from their NMR-derived 3D structures calculated in the absence of coupling based restraints. Solid line denotes the Karplus curve ($J(\phi) = A\cos^2(\phi–60) + B\cos(\phi–60) + C$; A = 6.63; B = –1.31; C = 1.63). The r.m.s.d. between measured and predicted couplings is ~0.9 Hz and ~1.0 Hz, respectively

new avenues for NMR-based studies of structure and folding of polypeptides. Further, the high yield of coupling information derived both in the case of predominantly β-sheet and α-helical proteins, indicates the feasibility of these experiments for medium to large size proteins.

Acknowledgements We gratefully acknowledge National Facility for High Field NMR at TIFR and NMR Research Center at IISc. We thank Dr. Y. Sharma, CCMB, Hyderabad and Prof. A. Bhattacharya, JNU, New Delhi for providing the expression systems for M-Crystallin and *Eh*-CaBP, respectively. HAS acknowledges DAE-BRNS Young Scientist Research Award.

References

Atreya HS, Sahu SC, Bhattacharya A, Chary KVR, Govil G (2001) NMR derived solution structure of an EF-Hand calcium-binding protein from *Entamoeba Histolytica*. Biochemistry 40:14392–14403

Atreya HS, Sahu SC, Chary KVR, Govil G (2000) A tracked approach for automated NMR assignments in proteins (TATAPRO). J Biomol NMR 17:125–136

Atreya HS, Szyperski T (2005) Rapid NMR data collection. Meth Enzymol 394:78–108

Baran MC, Huang YJ, Moseley HNB, Montelione G (2004) Automated analysis of protein NMR assignments and structures. Chem Rev 104:3541–3555

Barnwal RP, Jobby MK, Sharma Y, Chary KVR (2006) NMR assignment of M-crystallin: A novel Ca^{2+} binding protein of the $\beta\gamma$-crystallin superfamily from *Methanosarcina acetivorans*. J Biomol NMR 36(suppl):32

Biamonti C, Rios CB, Lyons B, Montelione G (1994) Multidimensional NMR experiments and analysis techniques for determining homo- and heteronuclear scalar coupling constants in proteins and nucleic acids. Adv Biophys Chem 4:51–120

Chary KVR, Otting G, Wüthrich K (1991) Measurement of small heteronuclear $^{1}H—^{15}N$ coupling constants in ^{15}N-labeled proteins by 3D H_NNH_{AB}-COSY. J Magn Reson 93:218–224

Choy WY, Sanctuary BC, Zhu G (1997) Using neural network predicted secondary structure information in automatic protein NMR assignment. J Chem Inf Comput Sci 37:1086–1094

Driscoll PC, Gronenborn A, Clore GM (1989) The influence of stereospecific assignments on the determination of three-dimensional structures of proteins by nuclear magnetic resonance spectroscopy: application to the sea anemone protein BDS-I. FEBS Lett 243:223–233

Dux P, Whitehead B, Boelens R, Kaptein R, Vuister GW (1997) Measurement of ^{15}N-^{1}H coupling constants in uniformly ^{15}N-labeled proteins: Application to the photoactive yellow protein. J Biomol NMR 10: 301–306

Dyson HJ, Wright PE (2004) Unfolded proteins and protein folding studied by NMR. Chem Rev 104:3607–3622

Freeman R (1998) Shaped radiofrequency pulses in high resolution NMR. Prog NMR Spectrosc 32:59–106

Garrett DS, Kuszewski J, Hancock TJ, Lodi PJ, Vuister GW, Gronenborn AM, Clore GM (1994) The impact of direct refinement against three-bond HN-CαH coupling constants on protein structure determination by NMR. J Magn Reson B 104:99–103

Güntert P, Braun W, Billeter M, Wüthrich K (1989) Automated stereospecific proton NMR assignments and their impact on the precision of protein structure determinations in solution. J Am Chem Soc 111:3997–4004

Karplus M (1963) Vicinal proton coupling in nuclear magnetic resonance. J Am Chem Soc 85:2870–2871

Kim S, Szyperski T (2003) GFT NMR, a new approach to rapidly obtain precise high-dimensional NMR spectral information. J Am Chem Soc 125:1385–1393

Kim YM, Prestegard JH (1990) Refinement of the NMR structures for acyl carrier protein with scalar coupling data. Proteins 8:377–385

Marion D, Ikura M, Tshudin R, Bax A (1989) Rapid recording of 2D NMR spectra without phase cycling: Application to the study of hydrogen exchange in proteins. J Magn Reson 85:393–399

Montelione GT, Zheng D, Huang YJ, Gunsalus KC, Szyperski TS (2000) Protein NMR spectroscopy in structural genomics. Nat Struct Mol Biol 7:982–985

Page R, Peti W, Wilson IA, Stevens RC, Wüthrich K (2005) NMR screening and crystal quality of bacterially expressed prokaryotic and eukaryotic proteins in a structural genomics pipeline. Proc Natl Acad Sci U S A 102:1901–1905

Pardi A, Billeter M, Wüthrich K (1984) Calibration of the angular dependence of the amide proton-C^{α} proton coupling constants, $^{3}J_{HN\alpha}$, in a globular protein. Use of $^{3}J_{HN\alpha}$ for identification of helical secondary structure. J Mol Biol 180:741–751

Piotto M, Saudek V, Sklenár V (1992) Gradient-tailored excitation for single-quantum NMR spectroscopy of aqueous solutions. J Biomol NMR 2:661–665

Shaka AJ, Barker PB, Freeman R (1985) Computer-optimized decoupling scheme for wideband applications and low-level operation. J Magn Reson 64:547–552

Szyperski T, Atreya HS (2006) Principles and applications of GFT projection NMR spectroscopy. Magn Reson Chem 44: S51–S60

Vuister GW, Bax A (1993) Quantitative J correlation: a new approach for measuring homonuclear three-bond $J(H^{N}H^{\alpha})$ coupling constants in ^{15}N-enriched proteins. J Am Chem Soc 115:7772–7777

Vuister GW, Grzesiek S, Delaglio F, Wang AC, Tschudin R, Zhu G, Bax A (1994) Measurement of homo- and heteronuclear J couplings from quantitative J correlation. Meth Enzymol 239:79–105

Wishart DS, Sykes BD (1994) Chemical shifts as a tool for structure determination. Meth Enzymol 239:363–392

Wüthrich K (1986) NMR of proteins and nucleic acids. Wiley, New York, pp 1–292